Modifying the Molecular Structure of Carbon Nanotubes through Gas-Phase Reactants

Citation: Michael J. Giannetto, Eric P. Johnson, Adam Watson, Edgar Dimitrov, Andrew Kurth, Wenbo Shi, Francesco Fornasiero, Eric R. Meshot, and Desiree L. Plata. ACS Nanoscience Au 2023 3 (2), 182-191.

Published Version: 10.1021/acsnanoscienceau.2c00052

Publisher: American Chemical Society

Permanent Link: https://hdl.handle.net/1721.1/153537

Version: Final published version: final published article, as it appeared in a journal, conference proceedings, or other formally published context

ACS NANOSCIENCE Au
AN OPEN ACCESS JOURNAL OF THE AMERICAN CHEMICAL SOCIETY

pubs.acs.org/nanoau Article

Modifying the Molecular Structure of Carbon Nanotubes through Gas-Phase Reactants

Michael J. Giannetto, Eric P. Johnson, Adam Watson, Edgar Dimitrov, Andrew Kurth, Wenbo Shi, Francesco Fornasiero, Eric R. Meshot, and Desiree L. Plata*

Cite This: *ACS Nanosci. Au* 2023, 3, 182–191 Read Online

ACCESS | Metrics & More | Article Recommendations | Supporting Information

ABSTRACT: Current approaches to carbon nanotube (CNT) synthesis are limited in their ability to control the placement of atoms on the surface of nanotubes. Some of this limitation stems from a lack of understanding of the chemical bond-building mechanisms at play in CNT growth. Here, we provide experimental evidence that supports an alkyne polymerization pathway in which short-chained alkynes directly incorporate into the CNT lattice during growth, partially retaining their side groups and influencing CNT morphology. Using acetylene, methyl acetylene, and vinyl acetylene as feedstock gases, unique morphological differences were observed. Interwall spacing, a highly conserved value in natural graphitic materials, varied to accommodate side groups, increasing systematically from acetylene to methyl acetylene to vinyl acetylene. Furthermore, attenuated total reflectance Fourier-transfer infrared spectroscopy (ATR-FTIR) illustrated the existence of intact methyl groups in the multiwalled CNTs derived from methyl acetylene. Finally, the nanoscale alignment of the CNTs grown in vertically aligned forests differed systematically. Methyl acetylene induced the most tortuous growth while CNTs from acetylene and vinyl-acetylene were more aligned, presumably due to the presence of polymerizable unsaturated bonds in the structure. These results demonstrate that feedstock hydrocarbons can alter the atomic-scale structure of CNTs, which in turn can affect properties on larger scales. This information could be leveraged to create more chemically and structurally complex CNT structures, enable more sustainable chemical pathways by avoiding the need for solvents and postreaction modifications, and potentially unlock experimental routes to a host of higher-order carbonaceous nanomaterials.

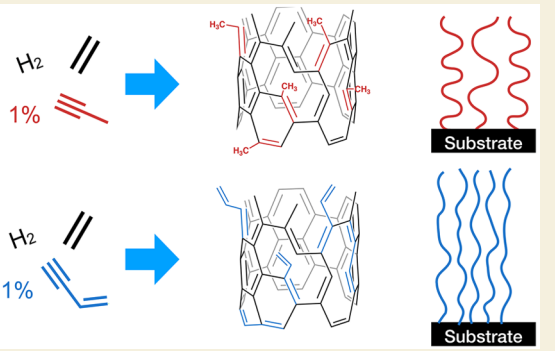

KEYWORDS: *carbon nanotube, alkyne, morphology, mechanism, acetylene, methyl acetylene, vinyl acetylene*

An improved mechanism for carbon nanotube (CNT) synthesis could simultaneously lower cost, enhance control, and reduce environmental impacts of production. CNT manufacturing remains an energy intensive and inefficient process, requiring 2−100 times more energy than aluminum production[1] and consuming resources at waste ratios equivalent to the pharmaceutical industry.[2] Large-scale synthesis techniques have poor selectivity and are unable to produce CNTs with tailored chemistries at high yields.[3] As a result, postsynthesis purification and functionalization processes are often utilized, and these reduce yield, increase resource consumption, and extend production time.[4] These factors contribute to high costs[5] and high cradle-to-gate environmental impacts,[6,7] preventing many CNT-enabled products from reaching the market[8] and potentially offsetting environmental benefits during the product's lifetime.[9] Identifying chemical bond-building mechanisms in CNT synthesis could help overcome these obstacles and enable more transformative CNT-based applications *while* reducing the environmental impacts of this expanding industry.[8,10−12]

The long-held understanding of CNT formation is that it occurs through the vapor−liquid−solid (VLS) and vapor−solid−solid (VSS) models.[13] VLS and VSS postulate that vapor-phase hydrocarbons thermally decompose and diffuse through a liquid or solid catalyst nanoparticle, and then precipitate on the surface as solid CNT.[14] Originally developed for solid Si whiskers[15] and then applied to carbonaceous materials,[16−19] these precipitation-based mechanisms have good experimental support but lack chemical detail and provide few "levers" with which to manipulate CNT structure.[20−22] Variations in the hydrocarbon composition of the feedstock gases[23,24] and the reactor environment[25] are known to affect CNT morphology, suggesting that thermal decomposition is not complete (e.g., to C_1 or C_2 units, as

Received: October 20, 2022
Revised: January 14, 2023
Accepted: January 18, 2023
Published: February 6, 2023

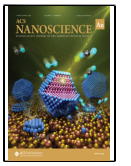

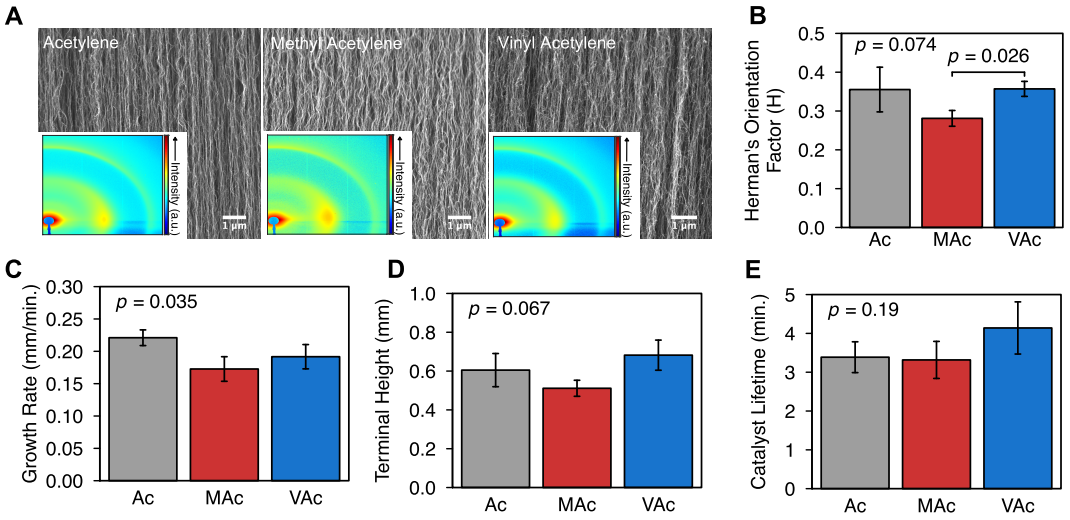

Figure 1. Alignment and growth analyses of CNT forests. (A) Representative SEM images taken from the side of CNT forests grown with either acetylene (Ac), methyl acetylene (MAc), or vinyl acetylene (VAc). Insets are synchrotron-based wide-angle X-ray scattering (WAXS) patterns of entire cross sections of these CNT forests. (B) Average Hermans orientation factor (H) values calculated from WAXS patterns of experimental triplicates. Error bars represent ±1 standard deviation. The p-value on the left was calculated from a one-way ANOVA across values from all three alkynes, while the p-value on the right comparing methyl acetylene CNTs and vinyl acetylene CNTs was calculated from a pairwise, two-tailed t test with Bonferroni correction. The other pairwise p-values were all much greater than 0.1 (SI Table S1). (C) Growth rates, (D) terminal heights, and (E) catalyst lifetimes of the CNT forests. (C and D calculated from growth curves in SI Figure S1). There are at least 3 experimental replicates for all analyses.

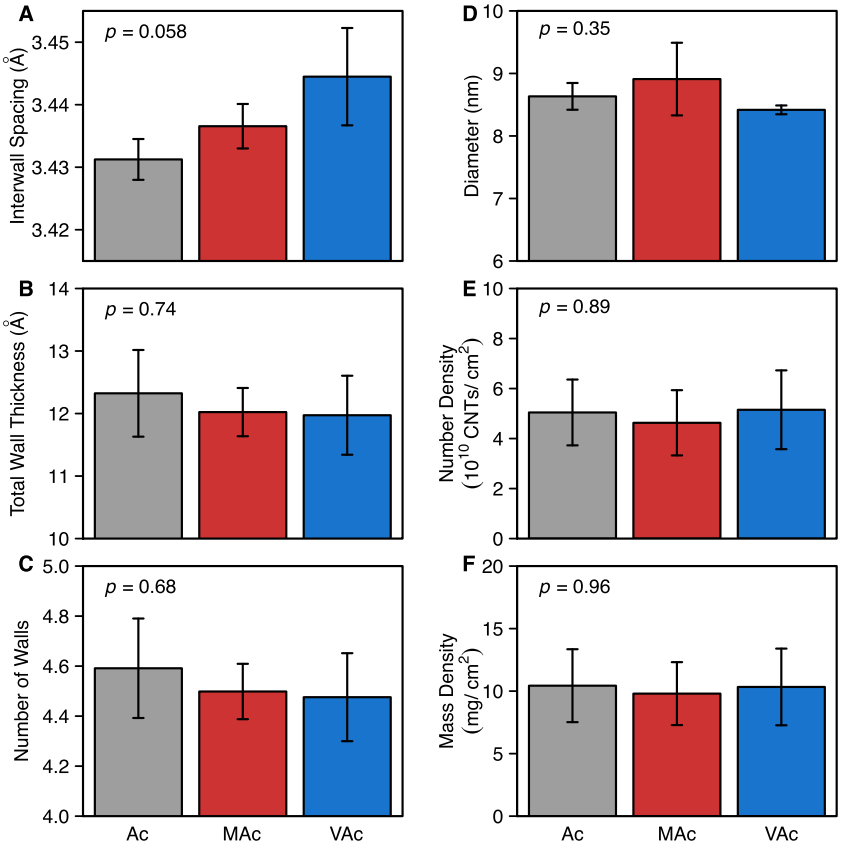

Figure 2. Atomic- and nanoscale properties determined by synchrotron-based X-ray scattering. (A) Interwall spacing between CNT walls and (B) total CNT wall thickness (outer diameter − inner diameter) as determined by WAXS. (C) Number of CNT walls was calculated from the interwall spacing and stack height (i.e., calculated from A and B). (D) CNT diameter, (E) number density throughout an array (i.e., calculated from D and F), and (F) mass density throughout an array as determined by small-angle X-ray scattering (SAXS) and X-ray attenuation. Error bars represent ±1 standard deviation of experimental triplicates. p-values were calculated with a one-way ANOVA across all three alkynes. Ac represents acetylene, MAc represents methyl acetylene, and VAc represents vinyl acetylene. Previous work has demonstrated that the outer wall CNT diameter is consistent with that of the supporting particle (Shi et al.[59]).

https://doi.org/10.1021/acsnanoscienceau.2c00052
ACS Nanosci. Au 2023, 3, 182−191

postulated by VLS/VSS).[26] Instead, incorporation of carbon via reaction with the catalyst surface[27,28] that bypasses complete decomposition of carbonaceous feedstock gases is possible.[29] Indeed, acetylene has been identified as a key precursor in CNT synthesis from multiple experimental and computational techniques.[30−34] Methyl acetylene, vinyl acetylene, and even hydrogen cyanide have displayed similar growth-enhancing abilities, suggesting that many short-chained alkynes could potentially participate in such direct-incorporation mechanisms.[35,36] Here, we sought to determine the effect of these varied alkynes on nanoscale structural differences in multiwalled CNT (MWCNT) forests grown in vertical alignment. If they persist, such differences would indicate that small alkynes are intact during CNT incorporation and carry their "cargo" with them, opening up potential for atomic-scale control in hierarchical nanomaterial structures.

Note that MWCNTs are a critical interrogation platform for the work presented here, as they have an additional parameter (interwall spacing) that can be probed. Further, MWCNTs and variations thereof (e.g., doubled walled nanotubes) have a broad application space[37] owing to their enhanced mechanical integrity and functionality (e.g., ability to functionalize the surface tube without compromise to conductivity of an inner tube). The chemical mechanisms presented here are relevant to nanotube growth for both single and multiwalled tubes, and the limitations that have faced scale up and control for both architectures may be informed by the below enumerated discoveries.

RESULTS AND DISCUSSION

Different Alkynes Affect Morphology in CNT Forests

Alkynes with different side groups (e.g., methyl or ethyl versus hydrogen) delivered to a resistively heated substrate induced morphological differences in CNT forests. SEM images of the sidewall of the forests suggested differences in alignment (Figure 1A), which was confirmed by X-ray scattering across billions of CNTs throughout the bulk of the forest. Hermans orientation factors, H, provide a measure of alignment, where 1 represents perfect vertical alignment, 0 is randomly oriented, and −0.5 is perfectly horizontal.[38,39] Calculated from X-ray scattering patterns, we find methyl acetylene (MAc)-derived CNTs were significantly less aligned than vinyl acetylene (VAc)-derived CNTs (H_{MAc} = 0.28 ± 0.02; H_{VAc} = 0.36 ± 0.02; p = 0.026, pairwise t test with Bonferroni correction), while the alignment of the acetylene (Ac) CNTs was statistically similar to both due the higher variation in acetylene-derived structures (H_{Ac} = 0.36 ± 0.06) (Figure 1B). H values ranging from 0.27 to 0.42 are typical of MWCNT forests,[39,40] and previous work has shown that alignment can be impacted by CNT number density[39] or external force exerted on the CNTs.[41] However, our forests had similar number densities (p = 0.89, ANOVA) (Figure 2E) and experienced similar mechanical forces (i.e., a silicon nitride cap) during growth. As such, differences in alignment must be associated with differences in chemical bond-building mechanisms. For example, acetylene moieties can engage in pi-back bonding with empty d-orbitals on the Fe catalyst[42] and participate in polymerization reactions (see SI Schematic S2); a terminal methyl group could frustrate this polymerization and result in persistent or dangling methyl groups protruding from the CNT lattice (as has been leveraged to direct the placement of methyl groups in ring formation reactions elsewhere[43−45]). Such persistence of a methyl group would result in defect formation and potential kinks in the lattice, giving rise to more tortuous structures in methyl acetylene-derived tubes. In contrast, vinyl acetylene is terminated with a double bond, which itself can participate in subsequent polymerization steps. Thus, the vinyl group can incorporate into the CNT sp^2 lattice, producing tubes with fewer defects and a higher degree of alignment. Acetylene presents an anomalous result, where alignment is good but highly variable (i.e., there is a larger relative standard error on the H), presumably due to the rapid reactivity of acetylene[46] (and higher growth rate; Figure 1C) either at the catalyst or via local thermal rearrangements creating a variety of alkenes and alkynes[36] that can react to form CNTs. Indeed, such a phenomenon may explain the anecdotal observation that hot-walled reactors tend to give more irregular and defective structures due to the myriad chemical reactants with which the catalyst can react.

The height displacement growth rate of the acetylene-derived forests was statistically faster than the methyl- and vinyl acetylene-derived forests (Figure 1C), whereas terminal height and catalyst lifetime displayed no significant differences (Figure 1D, E). Acetylene produced CNTs that grew roughly 30% and 15% faster than methyl acetylene and vinyl acetylene, respectively (p = 0.035, ANOVA). Here, we note that the we are reporting height change as a function of time, as measured by a laser displacement sensor, rather than CNT lengthening rate.[47,48] Calculating the lengthening rate from the orientation and height displacement gave consistent results, where acetylene produced CNTs that are formed 23% and 15% faster than methyl and vinyl acetylene, respectively (SI Table S2). As such, the growth rates should reflect real differences in chemical kinetics (i.e., reactivity at the catalyst) and diffusion. We note that diffusive differences would proceed in the order of acetylene, methyl acetylene, then vinyl acetylene (fastest to slowest), which was not observed. In contrast, the observed growth rate differences are consistent with coupled differences in alignment as well as chemical reactivity, both of which would operate in the same order and net effect (see detailed kinetic analysis in Figure S1, Figure S2, Figure S3, Table S2, and Table S3; briefly, we note that the system follows Michaelis−Menten kinetics observed in other catalyst-substrate systems). Taken together, these results support the existence of chemical differences in reactivity *and* the resultant nanoscale structures grown from a variety of short-chained alkynes, suggesting these molecules are intact during incorporation into a growing CNT lattice.

If methyl and vinyl group moieties are carried as "cargo" with the corresponding alkyne into CNT structures, rather than being removed prior to or simultaneously with incorporation at the catalyst, it is reasonable to expect that interwall spacing of the MWCNTs would increase from acetylene-, to methyl acetylene-, to vinyl acetylene-doped forests. This steady and statistically significant increase was observed, consistent with the existence of methyl and vinyl groups protruding from the CNT wall lattice throughout the MWCNT structure (Figure 2A; p-value = 0.058, ANOVA; n = 3 for each type). Considering the highly conserved interlayer spacing of graphitic materials in nature (around 3.4 Å),[49−55] the ability to tune this property with gaseous additives is noteworthy. There is precedent for altering this spacing in engineered materials: interlayer spacing between AB-stacked graphite has been reported at 3.335 Å, whereas turbostratic

https://doi.org/10.1021/acsnanoscienceau.2c00052
ACS Nanosci. Au 2023, 3, 182−191

and functionalized graphite have larger spacing to compensate for defects and extra atoms, ranging from 3.36−7.37 Å.[56,57] Strain in cylindrical graphitic structures can induce differences in interlayer spacing, where MWCNT interwall spacing has varied from 3.2 to 3.8 Å, varying inversely with tube diameter from 63.2 to 5.8 nm.[58] In our experiments, MWCNTs exhibited the same tube diameters across the different alkynes (Figure 2D) and could not explain the observed differences in MWCNT interwall spacing. Since we used a consistent annealing process (see SI) in all growths, all catalyst-controlled properties, such as number of walls, CNT diameter, number density, and mass density were conserved across the varied precursors (Figure 2B−F; $p > 0.1$). These parameters are largely determined by catalyst size and spacing,[59] which can be tuned with growth temperature,[60] annealing conditions,[61] oxidants in the feedstock,[62] or starting thickness of catalyst and support layer,[63,64] and have been shown to be unaffected by gas composition (i.e., trace alkynes doped in an ethylene, hydrogen, and helium atmosphere).[36] Therefore, controlling the reactive atmosphere during CNT growth provides a mode to independently modulate the atomic-scale structures of the tubes themselves while preserving other nanoscale and microscopic features of the material.

Chemical Differences via Vibrational Spectroscopy

Raman and attenuated total reflectance-Fourier transform infrared (FTIR) vibrational spectroscopies were used to probe the molecular defects and functional groups in as-grown CNT forests. Raman analysis revealed subtle yet significant differences in CNT defects between alkynes (Figure 3). A persistent shoulder was detected near the G band (approximately 1580 cm^{-1}) in the Raman spectra of acetylene- and methyl acetylene-fed CNTs, but was less prominent in vinyl acetylene-doped CNTs (Figure 3A). This shoulder at higher wavenumber (approximately 1620 cm^{-1}) is the D′ band,[65] which results from a double-resonant phonon scattering process associated with disruptions (i.e., defects) in graphitic networks.[56,66] Whereas the D band arises from *inter*valley resonance,[67] the D′ is due to *intra*valley resonance.[56,68] Unfortunately, it is difficult to translate this to specific structural information because defects can include a wide range of features such as caps, vacancies, heteroatoms, interstitial sites, and functionalization groups[69,70] (see SI for detailed discussion on the limitations of defect quantification via spectroscopic techniques and isotopic labeling approaches). Nevertheless, the D and D′ bands are each sensitive to different types of defects, again suggesting each alkyne gave rise to distinct atomic-scale features (see SI for further discussion). Additionally, the different trends observed in both intensity ratios (Figure 3B, C) and full-width half max (fwhm) values (Figure 3D) imply differences in defects between the alkyne-assisted CNTs.

The D/G ratio decreased significantly from 1.94 ± 0.09, to 1.67 ± 0.13, to 1.36 ± 0.05 for acetylene-, methyl acetylene-, and vinyl acetylene-doped CNTs, respectively (Figure 3B; $p = 8 \times 10^{-7}$, ANOVA), implying a decrease in certain types of defects. In contrast, the D′/G ratio was consistent between acetylene- and methyl acetylene-doped CNTs (0.58 ± 0.04 and 0.61 ± 0.08, respectively), but decreased significantly for vinyl acetylene-fed forests (to 0.42 ± 0.03; $p = 3 \times 10^{-4}$, ANOVA). Additionally, the fwhm of the D′ band is lower for vinyl acetylene CNTs than both acetylene and methyl acetylene CNTs, while the fwhm values of the G and D bands increased for vinyl acetylene CNTs (Figure 3C). This divergence of the fwhm values of vinyl acetylene CNTs further supports a difference in the defect type or density of the respective forests, but cannot be strictly interpreted as a unique feature with known structure.

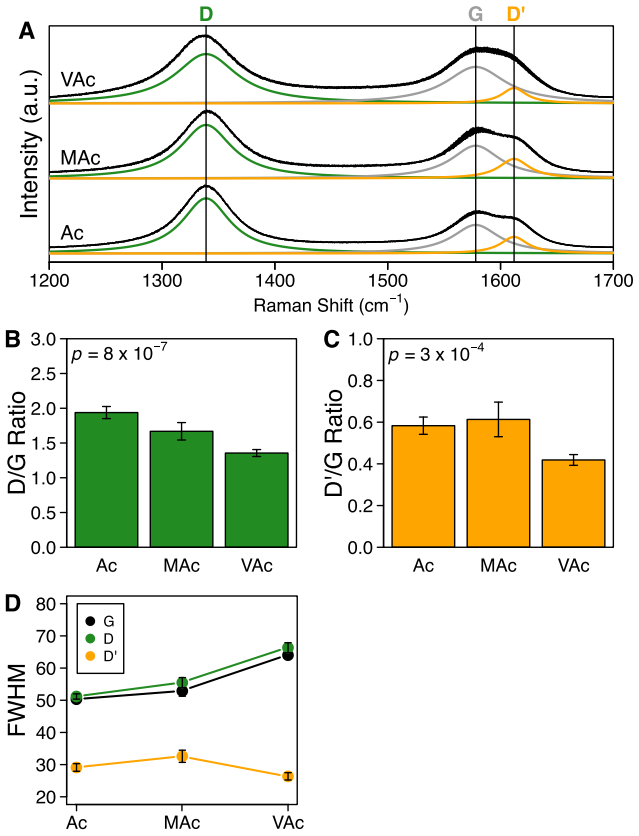

Figure 3. Raman spectroscopy reveals differences in defects among substituted alkyne-grown CNTs. (A) Raman spectra taken from the sidewalls of CNT forests. Black curves represent average spectral data of experimental triplicate forests, normalized to the height of the D band, and the thickness of the black curve represents ±1 standard deviation. The green, gray, and orange curves are the average Lorentzian fits to the D (1339 cm^{-1}), G (1578 cm^{-1}), and D′ (1612 cm^{-1}) bands, respectively. The vertical black lines indicate the average fitted peak location across all spectra. The fitted curves have been slightly separated, vertically, from the spectral data to aid with visualization. (B) D/G band and (C) D′/G band intensity ratios obtained from the Lorentzian fits (A). The *p*-values were calculated with a one-way ANOVA across experimental triplicates of all three alkynes. (D) Full-width half-max (fwhm; cm^{-1}) of the Lorentzian fits for the D, G, and D′ bands. All error bars in (B, C) represent ±1 standard deviation of experimental triplicates. Ac represents acetylene, MAc represents methyl acetylene, and VAc represents vinyl acetylene.

Thermogravimetric analysis (TGA) curves of experimental triplicates were nearly identical between alkynes, demonstrating no significant difference in onset or peak mass loss temperatures (average = 663 °C; $p = 0.93$, ANOVA) and no peaks at lower temperatures (SI Figure S4). Therefore, the observed differences in Raman results must be explained by bonding differences in the CNT lattice, rather than differences in total amounts of amorphous carbon. Finally, variations in D and D′ bands for vinyl acetylene CNTs are consistent with the alignment data (Figure 1B) that suggest the partial incorporation of vinyl groups from vinyl acetylene, resulting in fewer point defects. Nevertheless, some sp^2-C vinyl groups

https://doi.org/10.1021/acsnanoscienceau.2c00052
ACS Nanosci. Au 2023, 3, 182−191

necessarily protrude from the CNT walls to drive the larger interwall spacing (Figure 2A), giving rise to vinyl acetylene-related point defects that are distinct from those associated with by the sp^3-C methyl groups in methyl acetylene.

Evidence for the existence of persistent alkyne-associated side groups surviving into the CNT structure was observed via ATR-FTIR in the unique methyl-absorption bands associated with methyl-acetylene-doped CNTs (Figure 4). These spectra,

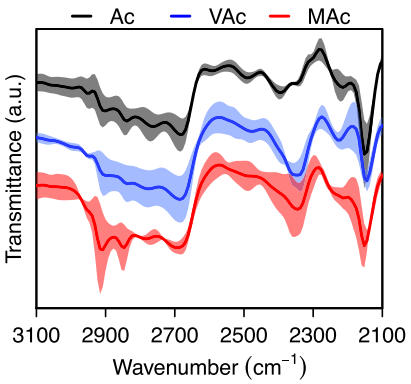

Figure 4. Methyl groups in methyl acetylene-grown CNTs detected in ATR-FTIR spectra of CNT forests. Dark, solid lines represent the average of experimental triplicates, while the shaded regions represent ±1 standard deviation. The peaks in the methyl acetylene-doped CNT spectra at 2915 and 2850 cm^{-1} are due to the asymmetric CH_2 stretching and symmetric CH_2 stretching vibrations, respectively.[71] A noteworthy feature at 2150 cm^{-1} is associated with alkynyl groups persistent in the solid structures. Ac represents acetylene, MAc represents methyl acetylene, and VAc represents vinyl acetylene.

taken from intact solids (i.e., no dispersants or sonication), were similar across all three alkynes except for the appearance of distinct features at 2915 and 2850 cm^{-1} in the methyl acetylene-grown CNTs. These absorptions are associated with asymmetric and symmetric sp^3 CH_2 vibrations in stretching modes, respectively,[71] and they have been associated with methyl groups in CNTs.[72,73] The unique features suggest that methyl groups are directly associated with methyl acetylene, implying that methyl acetylene incorporated directly into the CNT lattice (e.g., through a polymerization-like mechanism) rather than dissociating into carbon atoms or C_2 units that then assemble into CNTs in a random fashion. Interestingly, we did not observe any vinyl-associated absorptions in the spectra of vinyl acetylene-doped CNTs, such as $C{=}CH_2$ stretching modes at around 3000 cm^{-1}. This could either be due to masking of those features in the CNT structure (e.g., vinyl group density was below the detection limit of FTIR) or a result of the variable incorporation modes of the vinyl group on vinyl acetylene (see further discussion below. Also note that other experimental approaches may shed light on the existence of vinyl groups and ability of alkyne precursors to carry heteroatom moieties into growing CNT structures[74−76]). This versatility is plausible, as vinyl acetylene's double bond can take one of two different pathways: (1) protrude from the lattice, augmenting the interwall spacing (Figure 2A); or (2) react to incorporate cleanly into the CNT lattice (reducing tortuosity, Figure 1B, and defect density, Figure 3B, C). Regardless of the dominant mode, these results demonstrate that feedstock chemistry can be leveraged to alter CNT structure and bonding during the growth process. This *in situ*, gas-directed functionalization and atomic-scale manipulation has the potential to enable routes to a variety of previously inaccessible materials and has important implications for understanding how CNTs form on the molecular scale.

Additionally, a noteworthy feature observed at 2150 cm^{-1} is associated with alkynyl groups (i.e., triple bonds) persistent and common to all the solid CNT structures. This implies the existence of triple bonds in solid CNT structures, which is remarkable and suggests that common ball-and-stick models of CNTs (i.e., with all sp^2-hybridized, aromatic carbon rings) is incomplete. Other key differences between the spectra exist, but are difficult to attribute to precise chemical moieties in the structure due to a lack of peak attribution information (e.g., tabulated libraries or predicted IR features). These include the trimodal peaks between 2700 and 2400 cm^{-1} for Ac, but not VAc or MAc, an apparent shift of the peak at 2300 cm^{-1}, and an absorbing feature around 2350 cm^{-1} that is unique to MAc and Vac.

As a proof-of-concept demonstration (whose scalability and reproducibility remain to be determined), we illustrated how temporally varying the main alkyne precursor could give rise to unique morphological structure in a nanotube forest. Switching the alkyne precursors from acetylene to methyl acetylene resulted in a real-time change in the alignment of the nanotube forest (Figure 5; note that growth is from the bottom of the

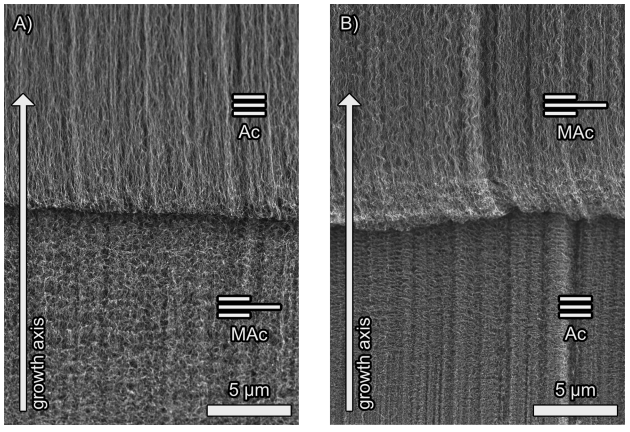

Figure 5. SEM image of the morphological evolution in forest sidewall at the junction where (A) acetylene was replaced by methyl acetylene and (B) methyl acetylene was replaced by acetylene.

forest in the upward direction), where more aligned structures appear at the top of the forest and more tortuous structures appear at the bottom. Conversely, adding methyl acetylene dopants first and then switching to acetylene causes a tortuous forest that is not able to fully recover its alignment, presumably due to disruption of the intertube mechanical forces necessary for good alignment in these mesoscale structures.[77] The potential for such structural tuning could be leveraged for a variety of hierarchically structured materials, ranging from size-exclusion membranes[78−81] to patterned interconnects that turn on demand, and beyond.

Implications

The morphological differences in CNTs generated from unique chemical reactants provides compelling evidence for a metal-mediated polymerization mechanism.[36,82] The structure of the short-chained (less than C_4) alkyne will influence the fate of the side group in what we introduce as "mixed-mode polymerization": alkynes with side groups lacking unsaturated

https://doi.org/10.1021/acsnanoscienceau.2c00052
ACS Nanosci. Au 2023, 3, 182−191

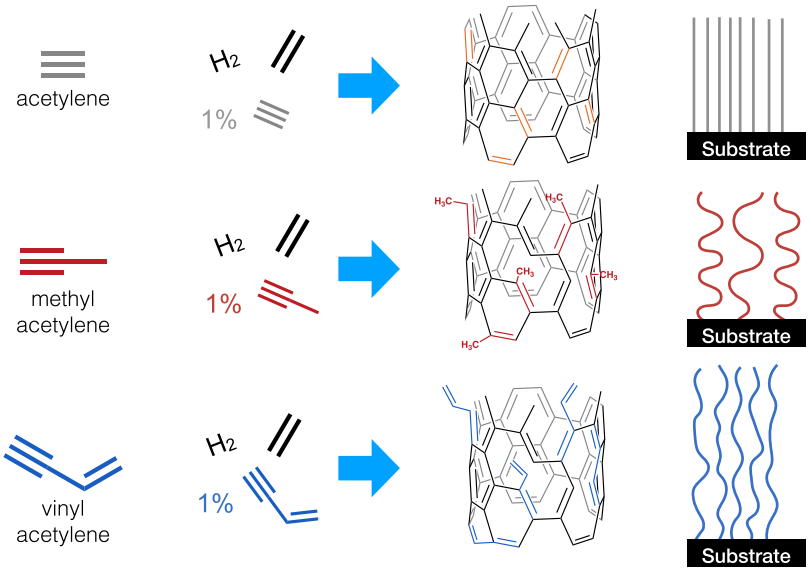

Figure 6. Variable alkynes exhibit unique influence on final nanotube structures mixed-mode polymerization, where unsaturated substituents on small alkynes (less than C4) can incorporate into a CNT lattice (forming sp^2 bonds) and saturated substitutes protrude from the lattice, introducing defects (or sp^3 bonding).

bonds (or pi-orbitals) will frustrate ring closure, leading to protruding side groups and more tortuous tubes, whereas alkynes with available pi-bonds may participate in rapid CNT polymerization *or* protrude from the CNT lattice (i.e., mixed-mode; Figure 6). Indeed, there is evidence that diacetylene (1,3-butadiyne; a "double acetylene" with an unsaturation as a "side group") gives rise to rapid CNT formation.[36,82,83] Understanding that alkynes react differently during CNT synthesis depending on the hybridization of their side group not only explains the variable atomic and nanoscale features observed here and in other work, but also helps one imagine chemical pathways to novel CNT structures. First, the observation that CNTs can be synthesized from a wide range of hydrocarbon fuels, where C/H ratios need to be optimized, is consistent with the common thermal generation of alkynes and their sensitivity to C/H loading.[82,84−87] Second, failure to achieve fully sp^2 nanotubes (i.e., those invoked by ball-and-stick imagery) is reconciled by acknowledgment that multiple alkynes are present in thermal reactive environments, and each of these is able to add to a building CNT structure, yielding more defective tubes. With this in mind, more attention must be paid to gaseous composition of the reactive atmosphere in order to achieve the degree of control sought for many applications (e.g., patterned interconnects or chiral control). Such data would also enable co-optimization of environmental performance via rigorous identification of volatile species concurrently with the synthetic optimization. Similarly, unreacted feedstocks could be appropriately filtered and recirculated to support subsequent CNT growth, greatly improving the product-to-waste ratios common to many synthetic approaches (other synthetic limitations to this approach are described in the referenced literature).[2,6,7,82,88,89] Finally, more accurate mechanistic models present an opportunity to unlock hierarchical nanocarbon structures with atomic-scale manipulation of features. This could include mechanical strength and electrical applications where nanotubes are covalently bonded at strategic locations or with epoxy resins (e.g., for stronger composites), patterned interconnects where curvature or turns in a continuous CNT are introduced through local switching of precursors (i.e., in pulsed molecular beam approaches), stacked forests where intertube spacing, alignment, and side groups vary throughout the height of the forest (e.g., to enable unique size exclusion applications), or covalently attaching heteroatoms that can serve as a link to other precise functionality (e.g., metals or metalloorganic substances). Such structures and their potential performance parameters are not often included in exploratory material databases constructed from computational models due to the large number of atoms and the associated computational complexity and power required.[90] However, those approaches are quickly becoming more efficient, and exploring the potential of these structures *in silico* could identify best-candidates for laboratory synthesis and functional performance corroboration. While these novel nanomaterials are still far from commercial-scale realization, the work presented here provides the chemical mechanistic understanding and practical approach for realization of those next-generation nanomaterials.

METHODS

CNT Synthesis

Vertically aligned multiwall CNT forests were grown in a cold-wall chemical vapor deposition (CVD) reactor (SI Schematic S1).[91] Si substrates (0.5 × 0.5 cm^2) layered with 10 nm Al_2O_3 and 1 nm Fe were used as the catalyst. Following an alkyne-assisted growth recipe,[36] CNT forests were grown at 650 °C and atmospheric pressure with 50% v/v H_2, 20% v/v ethylene, and 1% v/v of either acetylene, methyl acetylene, or vinyl acetylene, balanced with Ar to achieve a total flow rate of 604 sccm (standard cubic centimeters per minute; see SI for timing details).

A Keyence laser displacement sensor was used to monitor *in situ* height of the CNT forests.[60] Resulting growth curves of CNT forests were used to determine terminal height, linear growth rate, and catalyst lifetime.[60] Importantly, we note that vertically aligned forests are a model system allowing extraction of these growth kinetic parameters, and the chemical findings may extend to nonaligned nanotubes as well.

The alkyne-assisted growth method used here consistently produced CNT forests that covered the entire substrate. CNTs

https://doi.org/10.1021/acsnanoscienceau.2c00052
ACS Nanosci. Au 2023, 3, 182−191

reached their terminal heights of over 0.40 mm and in less than 5 min. All CNTs were of similar purity, according to thermogravimetric analysis (TGA) (SI Figure S4).

X-ray Analyses

Synchrotron-based small-angle X-ray scattering (SAXS; for nanoscale features) and wide-angle X-ray scattering (WAXS; for atomic scale features) were performed on CNT forests to collect quantitative morphological information averaged across billions of CNTs throughout the entire cross-section of the forest. Multiple scans were taken along the vertical height of the forests, and analyses were derived from spots with the maximum CNT number density. Degree of CNT alignment (or tortuosity) was assessed by calculating the Hermans orientation factor (H) from the X-ray scattering pattern intensity (I) along the azimuthal angle (ϕ) via the following equations:[92,93]

$$H = \frac{1}{2}(3\langle \cos^2 \phi \rangle - 1) \quad (1)$$

$$\langle \cos^{-2} \emptyset \rangle = \frac{\int_0^{\pi/2} I(\phi) \sin \phi \cos^2 \phi \, d\phi}{\int_0^{\pi/2} I(\phi) \sin \phi \, d\phi} \quad (2)$$

Average CNT diameter d was extracted from peak positions in SAXS I versus q curves ($d \sim 2\pi/q$),[39] where q is the scattering vector's magnitude. The average interwall spacing and wall thickness (i.e., graphene stack height) were determined from the peak position and width, respectively, in WAXS I vs q curves.[94,95] Mass density in a forest was determined from the attenuation of the X-ray intensity using the Beer–Lambert law.[96] The CNT number density was then calculated from the mass density values using the specific surface area of CNTs.[47] Wall number was calculated as stack height divided by interwall spacing plus 1.

CNT Characterization

In order to minimize the influence on CNT morphology and chemistry, CNTs forests were analyzed as-synthesized and not dispersed in solvent or sonicated. This is critically important because we sought to elucidate structural details of the as-grown forests. Preparative techniques required for some characterization, such as high-resolution transmission electron microscopy (HR-TEM), are known to induce structural changes. That is, the functional group attachments that we sought to image could be both induced or removed by the preparation procedure. As such, it would be unjustified to use HR-TEM as evidence that chemical functionality can be tuned with gas chemistry alone (i.e., the preparation technique is a chemical modification in and of itself). Thus, we exclusively characterized the materials using nondestructive techniques (see discussion and limitations to quantification in SI).

Scanning electron microscope analysis (SEM) (Hitachi SU-70) was conducted at 10 000 magnification on the side of CNT forests 0.1 mm above the substrate at multiple locations (representative images in Figure 1A).

Raman spectra from 1200 to 1700 cm^{-1} were taken with a Horiba LabRAM HR Evolution by focusing a 532 nm laser on the side of CNT forests. Three different spots on the same face of each forest were analyzed and averaged. A line was drawn between the two end points of the spectra and subtracted out to zero the tails. Then, each spectra was normalized to its respective D band (1339 cm^{-1}) height to facilitate observation of differences in the G (1578 cm^{-1}) and D′ (1612 cm^{-1}) bands.[97] Finally, we fit these bands with three separate Lorentzian curves[98,99] using the nonlinear least-squares (nls) function in R. Peak height and full-width half-maximum (fwhm) values were taken from the fitted curves. Averages and standard deviations were calculated from the zeroed and normalized spectra of experimental triplicates.

ATR-FTIR was used to detect bonding differences between CNT forests grown with different alkynes. As-synthesized CNTs were scraped off of their substrate directly onto the ATR crystal in an approximately even coating, and pressed with an anvil to ensure direct contact with the crystal. Spectra were collected in transmission mode and normalized to a 101-point moving average of the original data. Averages and standard deviations were calculated from spectra of experimental triplicates.

All analyses were conducted on experimental triplicates from three separate growths from each alkyne. Values in the text are reported as the mean of experimental triplicates, plus or minus one standard deviation. All data processing and statistical analyses were conducted in R, and statistical significance was defined as p values below 0.05. All pairwise t tests with Bonferroni correction (to reduce the chances of Type I error that increases from multiple tests of hypotheses[100]) are available in SI Table S1.

ASSOCIATED CONTENT

Supporting Information

The Supporting Information is available free of charge at https://pubs.acs.org/doi/10.1021/acsnanoscienceau.2c00052.

Detailed materials and methods description; schematic of cold-wall reactor; growth curves of alkynes and detailed kinetic analysis; thermogravimetric analysis of CNTs; SEM images of CNTs; p-values from all pairwise t tests with Bonferroni correction; proposed reaction mechanisms (PDF)

AUTHOR INFORMATION

Corresponding Author

Desiree L. Plata − *Department of Civil and Environmental Engineering, Massachusetts Institute of Technology, Cambridge, Massachusetts 02139, United States; Department of Chemical and Environmental Engineering, Yale University, New Haven, Connecticut 06511, United States;* orcid.org/0000-0003-0657-7735; Email: dplata@mit.edu

Authors

Michael J. Giannetto − *Department of Chemical and Environmental Engineering, Yale University, New Haven, Connecticut 06511, United States*

Eric P. Johnson − *Department of Chemical and Environmental Engineering, Yale University, New Haven, Connecticut 06511, United States; Department of Civil and Environmental Engineering, Massachusetts Institute of Technology, Cambridge, Massachusetts 02139, United States;* orcid.org/0000-0003-2214-2977

Adam Watson − *Department of Chemical and Environmental Engineering, Yale University, New Haven, Connecticut 06511, United States*

Edgar Dimitrov − *Department of Physics, University of California, Berkeley, Berkeley, California 94720, United States;* Present Address: Department of Physics, Pennsylvania State University, State College, Pennsylvania 18601, United States

Andrew Kurth − *Department of Chemical and Environmental Engineering, Yale University, New Haven, Connecticut 06511, United States*

Wenbo Shi − *Department of Civil and Environmental Engineering, Massachusetts Institute of Technology, Cambridge, Massachusetts 02139, United States*

Francesco Fornasiero − *Physical and Life Sciences Directorate, Lawrence Livermore National Laboratory, Livermore, California 94550, United States;* orcid.org/0000-0002-3505-5867

https://doi.org/10.1021/acsnanoscienceau.2c00052
ACS Nanosci. Au 2023, 3, 182−191

Eric R. Meshot − *Physical and Life Sciences Directorate, Lawrence Livermore National Laboratory, Livermore, California 94550, United States;* orcid.org/0000-0002-7951-6696

Complete contact information is available at: https://pubs.acs.org/10.1021/acsnanoscienceau.2c00052

Author Contributions

D.L.P. and E.R.M. conceived the ideas, designed the study, and supervised the project; M.J.G., E.P.J., A.W., A.K., E.D., E.R.M., and W.S. designed and performed experiments; M.J.G., E.P.J., E.D., and E.R.M analyzed data; D.L.P. and M.J.G. wrote the manuscript.

Notes

The authors declare no competing financial interest.

■ ACKNOWLEDGMENTS

This work was supported by NSF Award Number 1552993, EPA grant number RD835580, and Yale University graduate fellowships. We thank Dr. M. Rooks for assistance with shared facilities at the Yale Institute for Nanoscience and Quantum Engineering (YINQE). A portion of this work was performed under the auspices of the U.S. Department of Energy by Lawrence Livermore National Laboratory under Contract DE-AC52-07NA27344 with support from the Laboratory Directed Research and Development (LDRD) Program under project 21-ERD-024. The Advanced Light Source (ALS) (Beamline 7.3.3) is supported by the Office of Science, Office of Basic Energy Sciences, of the U.S. Department of Energy under contract no. DE-AC02-05CH11231. Part of this work was enabled by the financial support from the Defense Threat Reduction Agency (DTRA-CB) via grant BA12PHM123.

■ REFERENCES

(1) Kushnir, D.; Sandén, B. A. Energy Requirements of Carbon Nanoparticle Production. *J. Ind. Ecol* **2008**, *12*, 360−375.
(2) Eckelman, M. J.; Zimmerman, J. B.; Anastas, P. T. Toward Green Nano: E-Factor Analysis of Several Nanomaterial Syntheses. *J. Ind. Ecol* **2008**, *12* (3), 316−328.
(3) Rao, R.; Pint, C. L.; Islam, A. E.; Weatherup, R. S.; Hofmann, S.; Meshot, E. R.; Wu, F.; Zhou, C.; Dee, N.; Amama, P. B.; Carpena-Nuñez, J.; Shi, W.; Plata, D. L.; Penev, E. S.; Yakobson, B. I.; Balbuena, P. B.; Bichara, C.; Futaba, D. N.; Noda, S.; Shin, H.; Kim, K. S.; Simard, B.; Mirri, F.; Pasquali, M.; Fornasiero, F.; Kauppinen, E. I.; Arnold, M.; Cola, B. A.; Nikolaev, P.; Arepalli, S.; Cheng, H.-M.; Zakharov, D. N.; Stach, E. A.; Zhang, J.; Wei, F.; Terrones, M.; Geohegan, D. B.; Maruyama, B.; Maruyama, S.; Li, Y.; Adams, W. W.; Hart, A. J. Carbon Nanotubes and Related Nanomaterials: Critical Advances and Challenges for Synthesis toward Mainstream Commercial Applications. *ACS Nano* **2018**, *12* (12), 11756−11784.
(4) Hou, P. X.; Liu, C.; Cheng, H. M. Purification of Carbon Nanotubes. *Carbon* **2008**, *46* (15), 2003−2025.
(5) Isaacs, J. A.; Tanwani, A.; Healy, M. L.; Dahlben, L. J. Economic Assessment of Single-Walled Carbon Nanotube Processes. *J. Nanoparticle Res.* **2010**, *12*, 551−562.
(6) Eckelman, M. J.; Mauter, M. S.; Isaacs, J. A.; Elimelech, M. New Perspectives on Nanomaterial Aquatic Ecotoxicity: Production Impacts Exceed Direct Exposure Impacts for Carbon Nanotoubes. *Environ. Sci. Technol.* **2012**, *46* (5), 2902−2910.
(7) Healy, M. L.; Dahlben, L. J.; Isaacs, J. A. Environmental Assessment of Single-Walled Carbon Nanotube Processes. *J. Ind. Ecol* **2008**, *12* (3), 376−393.
(8) De Volder, M. F. L.; Tawfick, S. H.; Baughman, R. H.; Hart, A. J. Carbon Nanotubes: Present and Future Commercial Applications. *Science* **2013**, *339* (6119), 535−539.
(9) Zhai, P.; Isaacs, J. A.; Eckelman, M. J. Net Energy Benefits of Carbon Nanotube Applications. *Appl. Energy* **2016**, *173*, 624−634.
(10) See, C. H.; Harris, A. T. A Review of Carbon Nanotube Synthesis via Fluidized-Bed Chemical Vapor Deposition. *Ind. Eng. Chem. Res.* **2007**, *46* (4), 997−1012.
(11) Gilbertson, L. M.; Zimmerman, J. B.; Plata, D. L.; Hutchison, J. E.; Anastas, P. T. Designing Nanomaterials to Maximize Performance and Minimize Undesirable Implications Guided by the Principles of Green Chemistry. *Chem. Soc. Rev.* **2015**, *44* (16), 5758−5777.
(12) Hills, G.; Lau, C.; Wright, A.; Fuller, S.; Bishop, M. D.; Srimani, T.; Kanhaiya, P.; Ho, R.; Amer, A.; Stein, Y.; et al. Modern Microprocessor Built from Complementary Carbon Nanotube Transistors. *Nature* **2019**, *572*, 595−602.
(13) Parker, J. M.; Wong, H. S. P. Synergetic Carbon Nanotube Growth. *Carbon N. Y* **2013**, *62*, 61−68.
(14) Tessonnier, J. P.; Su, D. S. Recent Progress on the Growth Mechanism of Carbon Nanotubes: A Review. *ChemSusChem* **2011**, *4* (7), 824−847.
(15) Wagner, R. S.; Ellis, W. C. Vapor-Liquid-Solid Mechanism of Single Crystal Growth. *Appl. Phys. Lett.* **1964**, *4* (5), 89.
(16) Baker, R. T. K.; Barber, M. A.; Harris, P. S.; Feates, F. S.; Waite, R. J. Nucleation and Growth of Carbon Deposits from the Nickel Catalyzed Decomposition of Acetylene. *J. Catal.* **1972**, *26* (1), 51−62.
(17) Baker, R. T. K.; Harris, P. S.; Thomas, R. B.; Waite, R. J. Formation of Filamentous Carbon from Iron, Cobalt and Chromium Catalyzed Decomposition of Acetylene. *J. Catal.* **1973**, *30* (1), 86−95.
(18) Sinnott, S. B.; Andrews, R.; Qian, D.; Rao, A. M.; Mao, Z.; Dickey, E. C.; Derbyshire, F. Model of Carbon Nanotube Growth through Chemical Vapor Deposition. *Chem. Phys. Lett.* **1999**, *315* (1−2), 25−30.
(19) Kukovitsky, E. F.; L'Vov, S. G.; Sainov, N. A. VLS-Growth of Carbon Nanotubes from the Vapor. *Chem. Phys. Lett.* **2000**, *317* (1−2), 65−70.
(20) Baker, R. T. K. Catalytic Growth of Carbon Filaments. *Carbon N. Y* **1989**, *27* (3), 315−323.
(21) Baird, T.; Fryer, J. R.; Grant, B. Carbon Formation on Iron and Nickel Foils by Hydrocarbon Pyrolysis-Reactions at 700°C. *Carbon N. Y* **1974**, *12* (5), 591−602.
(22) Reilly, P. T. A.; Whitten, W. B. The Role of Free Radical Condensates in the Production of Carbon Nanotubes during the Hydrocarbon CVD Process. *Carbon N. Y* **2006**, *44* (9), 1653−1660.
(23) Li, Q.; Yan, H.; Zhang, J.; Liu, Z. Effect of Hydrocarbons Precursors on the Formation of Carbon Nanotubes in Chemical Vapor Deposition. *Carbon N. Y* **2004**, *42* (4), 829−835.
(24) Shaikjee, A.; Coville, N. J. The Effect of Substituted Alkynes on Nickel Catalyst Morphology and Carbon Fiber Growth. *Carbon N. Y* **2012**, *50* (3), 1099−1108.
(25) Youn, S. K.; Frouzakis, C. E.; Gopi, B. P.; Robertson, J.; Teo, K. B. K.; Park, H. G. Temperature Gradient Chemical Vapor Deposition of Vertically Aligned Carbon Nanotubes. *Carbon N. Y* **2013**, *54*, 343−352.
(26) Khalilov, U.; Bogaerts, A.; Neyts, E. C. Atomic Scale Simulation of Carbon Nanotube Nucleation from Hydrocarbon Precursors. *Nat. Commun.* **2015**, *6*, 10306.
(27) Penev, E. S.; Bets, K. V.; Gupta, N.; Yakobson, B. I. Transient Kinetic Selectivity in Nanotubes Growth on Solid Co-W Catalyst. *Nano Lett.* **2018**, *18* (8), 5288−5293.
(28) Eres, G.; Rouleau, C. M.; Yoon, M.; Puretzky, A. A.; Jackson, J. J.; Geohegan, D. B. Model for Self-Assembly of Carbon Nanotubes from Acetylene Based on Real-Time Studies of Vertically Aligned Growth Kinetics. *J. Phys. Chem. C* **2009**, *113* (35), 15484−15491.
(29) Liu, K.; Jiang, K.; Feng, C.; Chen, Z.; Fan, S. A Growth Mark Method for Studying Growth Mechanism of Carbon Nanotube Arrays. *Carbon N. Y* **2005**, *43* (14), 2850−2856.
(30) Sugime, H.; Noda, S. Cold-Gas Chemical Vapor Deposition to Identify the Key Precursor for Rapidly Growing Vertically-Aligned

Single-Wall and Few-Wall Carbon Nanotubes from Pyrolyzed Ethanol. *Carbon N. Y* **2012**, *50* (8), 2953−2960.
(31) Eres, G.; Kinkhabwala, A. A.; Cui, H.; Geohegan, D. B.; Puretzky, A. A.; Lowndes, D. H. Molecular Beam-Controlled Nucleation and Growth of Vertically Aligned Single-Wall Carbon Nanotube Arrays. *J. Phys. Chem. B* **2005**, *109* (35), 16684−16694.
(32) Kimura, H.; Goto, J.; Yasuda, S.; Sakurai, S.; Yumura, M.; Futaba, D. N.; Hata, K. Unexpectedly High Yield Carbon Nanotube Synthesis from Low-Activity Carbon Feedstocks at High Concentrations. *ACS Nano* **2013**, *7* (4), 3150−3157.
(33) Shi, W.; Xue, K.; Meshot, E. R.; Plata, D. L. The Carbon Nanotube Formation Parameter Space: Data Mining and Mechanistic Understanding for Efficient Resource Use. *Green Chem.* **2017**, *19* (16), 3787−3800.
(34) Wang, Y.; Gao, X.; Qian, H. J.; Ohta, Y.; Wu, X.; Eres, G.; Morokuma, K.; Irle, S. Quantum Chemical Simulations Reveal Acetylene-Based Growth Mechanisms in the Chemical Vapor Deposition Synthesis of Carbon Nanotubes. *Carbon N. Y* **2014**, *72*, 22−37.
(35) Pint, C. L.; Sun, Z.; Moghazy, S.; Xu, Y.-Q.; Tour, J. M.; Hauge, R. H. Supergrowth of Nitrogen-Doped Single-Walled Carbon Nanotube Arrays: Active Species, Dopant Characterization, and Doped/Undoped Heterojunctions. *ACS Nano* **2011**, *5* (9), 6925−6934.
(36) Plata, D. L.; Meshot, E. R.; Reddy, C. M.; Hart, A. J.; Gschwend, P. M. Multiple Alkynes React with Ethylene to Enhance Carbon Nanotube Synthesis, Suggesting a Polymerization-like Formation Mechanism. *ACS Nano* **2010**, *4* (12), 7185−7192.
(37) Janković, N. Z.; Plata, D. L. Engineered Nanomaterials in the Context of Global Element Cycles. *Environ. Sci. Nano* **2019**, *6* (9), 2697−2711.
(38) Hermans, J. J.; Hermans, P. H.; Vermaas, D.; Weidinger, A. Quantitative Evaluation of Orientation in Cellulose Fibres from the X-ray Fibre Diagram. *Recl. des Trav. Chim. des Pays-Bas* **1946**, *65* (6), 427−447.
(39) Meshot, E. R.; Zwissler, D. W.; Bui, N.; Kuykendall, T. R.; Wang, C.; Hexemer, A.; Wu, K. J. J.; Fornasiero, F. Quantifying the Hierarchical Order in Self-Aligned Carbon Nanotubes from Atomic to Micrometer Scale. *ACS Nano* **2017**, *11* (6), 5405−5416.
(40) Li, J.; Bedewy, M.; White, A. O.; Polsen, E. S.; Tawfick, S.; Hart, A. J. Highly Consistent Atmospheric Pressure Synthesis of Carbon Nanotube Forests by Mitigation of Moisture Transients. *J. Phys. Chem. C* **2016**, *120* (20), 11277−11287.
(41) Hart, A. J.; Slocum, A. H. Force Output, Control of Film Structure, and Microscale Shape Transfer by Carbon Nanotube Growth under Mechanical Pressure. *Nano Lett.* **2006**, *6* (6), 1254−1260.
(42) House, J. E.; House, K. A.*Descriptive Inorganic Chemistry*, 2nd ed.; Elsevier: Burlington, MA, 2010.
(43) Choi, K. Y.; Ray, W. H. Polymerization of Olefins through Heterogeneous Catalysis. II. Kinetics of Gas Phase Propylene Polymerization with Ziegler−Natta Catalysts. *J. Appl. Polym. Sci.* **1985**, *30* (3), 1065−1081.
(44) Jaber, I. A.; Ray, W. H. Polymerization of Olefins through Heterogeneous Catalysis. XIV. The Influence of Temperature in the Solution Copolymerization of Ethylene. *J. Appl. Polym. Sci.* **1993**, *50* (2), 201−215.
(45) Jaber, I. A.; Ray, W. H. Polymerization of Olefins through Heterogeneous Catalysis. XV. The Influence of Pressure in the Solution Copolymerization of Ethylene. *J. Appl. Polym. Sci.* **1993**, *50* (2), 217−231.
(46) Rao, R.; Liptak, D.; Cherukuri, T.; Yakobson, B. I.; Maruyama, B. In Situ Evidence for Chirality-Dependent Growth Rates of Individual Carbon Nanotubes. *Nat. Mater.* **2012**, *11* (3), 213−216.
(47) Esconjauregui, S.; Xie, R.; Fouquet, M.; Cartwright, R.; Hardeman, D.; Yang, J.; Robertson, J. Measurement of Area Density of Vertically Aligned Carbon Nanotube Forests by the Weight-Gain Method. *J. Appl. Phys.* **2013**, *113*, 144309.
(48) Meshot, E. R.; Bedewy, M.; Lyons, K. M.; Woll, A. R.; Juggernauth, K. A.; Tawfick, S.; Hart, A. J. Measuring the Lengthening Kinetics of Aligned Nanostructures by Spatiotemporal Correlation of Height and Orientation. *Nanoscale* **2010**, *2*, 896−900.
(49) Goldberg, E. D.*Black Carbon in the Environment: Properties and Distribution*; Wiley and Sons, New York, 1985.
(50) Zhang, Z.; Zhang, W.; Awad, O. I.; Ma, X.; Pan, S.; Xu, H.; Shuai, S. Improved HRTEM Image Processing Methods and the Application on Soot Nanostructure Analysis for GDI Engine. *Fuel* **2020**, *267*, 116974.
(51) Toth, P.; Palotas, A. B.; Eddings, E. G.; Whitaker, R. T.; Lighty, J. S. A Novel Framework for the Quantitative Analysis of High Resolution Transmission Electron Micrographs of Soot I. Improved Measurement of Interlayer Spacing. *Combust. Flame* **2013**, *160* (5), 909−919.
(52) Palotas, A. B.; Rainey, L. C.; Sarofim, A.; Vander Sande, J. B.; Flagan, R. C. Where Did That Soot Come From? *CHEMTECH* **1998**, *28* (7), 24−30.
(53) Palotás, Á. B.; Rainey, L. C.; Feldermann, C. J.; Sarofim, A. F.; Vander Sande, J. B. Soot Morphology: An Application of Image Analysis in High-Resolution Transmission Electron Microscopy. *Microsc. Res. Tech* **1996**, *33* (3), 266−278.
(54) Sharma, A.; Kyotani, T.; Tomita, A. A New Quantitative Approach for Microstructural Analysis of Coal Char Using HRTEM Images. *Fuel* **1999**, *78* (10), 1203−1212.
(55) Yehliu, K.; Vander Wal, R. L.; Boehman, A. L. A Comparison of Soot Nanostructure Obtained Using Two High Resolution Transmission Electron Microscopy Image Analysis Algorithms. *Carbon N. Y* **2011**, *49* (13), 4256−4268.
(56) Pimenta, M. A.; Dresselhaus, G.; Dresselhaus, M. S.; Cançado, L. G.; Jorio, A.; Saito, R. Studying Disorder in Graphite-Based Systems by Raman Spectroscopy. *Phys. Chem. Chem. Phys.* **2007**, *9*, 1276−1290.
(57) Jeong, H.-K.; Lee, Y. P.; Lahaye, R. J. W. E.; Park, M.-H.; An, K. H.; Kim, I. J.; Yang, C.-W.; Park, C. Y.; Ruoff, R. S.; Lee, Y. H. Evidence of Graphitic AB Stacking Order of Graphite Oxides. *J. Am. Chem. Soc.* **2008**, *130* (4), 1362−1366.
(58) Singh, D. K.; Iyer, P. K.; Giri, P. K. Diameter Dependence of Interwall Separation and Strain in Multiwalled Carbon Nanotubes Probed by X-Ray Diffraction and Raman Scattering Studies. *Diam. Relat. Mater.* **2010**, *19* (10), 1281−1288.
(59) Shi, W.; Li, J.; Polsen, E. S.; Oliver, C. R.; Zhao, Y.; Meshot, E. R.; Barclay, M.; Fairbrother, D. H.; Hart, A. J.; Plata, D. L. Oxygen-Promoted Catalyst Sintering Influences Number Density, Alignment, and Wall Number of Vertically Aligned Carbon Nanotubes. *Nanoscale* **2017**, *9* (16), 5222−5233.
(60) Meshot, E. R.; Plata, D. L.; Tawfick, S.; Zhang, Y.; Verploegen, E. A.; Hart, A. J. Engineering Vertically Aligned Carbon Nanotube Growth by Decoupled Thermal Treatment of Precursor and Catalyst. *ACS Nano* **2009**, *3* (9), 2477−2486.
(61) Sakurai, S.; Inaguma, M.; Futaba, D. N.; Yumura, M.; Hata, K. Diameter and Density Control of Single-Walled Carbon Nanotube Forests by Modulating Ostwald Ripening through Decoupling the Catalyst Formation and Growth Processes. *Small* **2013**, *9* (21), 3584−3592.
(62) Li, Y.; Xu, G.; Zhang, H.; Li, T.; Yao, Y.; Li, Q.; Dai, Z. Alcohol-Assisted Rapid Growth of Vertically Aligned Carbon Nanotube Arrays. *Carbon N. Y* **2015**, *91*, 45−55.
(63) Zhong, G. F.; Iwasaki, T.; Kawarada, H. Semi-Quantitative Study on the Fabrication of Densely Packed and Vertically Aligned Single-Walled Carbon Nanotubes. *Carbon N. Y* **2006**, *44* (10), 2009−2014.
(64) Mattevi, C.; Wirth, C. T.; Hofmann, S.; Blume, R.; Cantoro, M.; Ducati, C.; Cepek, C.; Knop-Gericke, A.; Milne, S.; Castellarin-Cudia, C.; Dolafi, S.; Goldoni, A.; Schloegl, R.; Robertson, J. In-Situ X-Ray Photoelectron Spectroscopy Study of Catalyst-Support Interactions and Growth of Carbon Nanotube Forests. *J. Phys. Chem. C* **2008**, *112* (32), 12207−12213.

https://doi.org/10.1021/acsnanoscienceau.2c00052
ACS Nanosci. Au 2023, 3, 182−191

(65) Jorio, A; Pimenta, M A; Filho, A G S.; Saito, R; Dresselhaus, G; Dresselhaus, M S Characterizing Carbon Nanotube Samples with Resonance Raman Scattering. *New J. Phys.* **2003**, *5*, 139.
(66) Cançado, L. G.; Jorio, A.; Pimenta, M. A. Measuring the Absolute Raman Cross Section of Nanographites as a Function of Laser Energy and Crystallite Size. *Phys. Rev. B - Condens. Matter Mater. Phys.* **2007**, *76*, 064304.
(67) Saito, R.; Jorio, A.; Souza Filho, A. G.; Dresselhaus, M. S.; Dresselhaus, G.; Pimenta, M. A. Probing Phonon Dispersion Relations of Graphite by Double Resonance Raman Scattering. *Phys. Rev. Lett.* **2001**, *88*, 027401.
(68) Cançado, L. G.; Pimenta, M. A.; Neves, B. R. A.; Dantas, M. S. S.; Jorio, A. Influence of the Atomic Structure on the Raman Spectra of Graphite Edges. *Phys. Rev. Lett.* **2004**, *93*, 247401.
(69) Chakrapani, N.; Curran, S.; Wei, B.; Ajayan, P. M.; Carrillo, A.; Kane, R. S. Spectral Fingerprinting of Structural Defects in Plasma-Treated Carbon Nanotubes. *J. Mater. Res.* **2003**, *18*, 2515−2521.
(70) Narlikar, A. V.; Fu, Y. Y.*Oxford Handbook of Nanoscience and Technology: Frontiers and Advances*; Oxford University Press, 2010; pp 31−93.
(71) Heitz, T.; Drévillon, B.; Godet, C.; Bourée, J. Quantitative Study of C—H Bonding in Polymerlike Amorphous Carbon Films Using in Situ Infrared Ellipsometry. *Phys. Rev. B - Condens. Matter Mater. Phys.* **1998**, *58*, 13957.
(72) Zhang, G.; Qi, P.; Wang, X.; Lu, Y.; Li, X.; Tu, R.; Bangsaruntip, S.; Mann, D.; Zhang, L.; Dai, H. Selective Etching of Metallic Carbon Nanotubes by Gas-Phase Reaction. *Science* **2006**, *314* (5801), 974−977.
(73) Saini, R. K.; Chiang, I. W.; Peng, H.; Smalley, R. E.; Billups, W. E.; Hauge, R. H.; Margrave, J. L. Covalent Sidewall Functionalization of Single Wall Carbon Nanotubes. *J. Am. Chem. Soc.* **2003**, *125* (12), 3617−3612.
(74) Johnson, E. P.; Shi, W.; Plata, D. L. Oxygen-Functionalized Alkyne Precursors in Carbon Nanotube Growth. *MRS Bull.* **2021**, *46* (6), 471−480.
(75) Johnson, E. P.Gas-Phase Control of Heteroatom Placement and Structure in Carbon Nanotube Synthesis. *PhD Thesis*; Yale University, New Haven, CT, 2022.
(76) Johnson, E. P.; Aquino de Carvalho, N.; Gilbertson, L. M.; Plata, D. L.Acid Treatment in Alkyl-Functionalized Carbon Nanotubes: Chemical Insights and Environmental Applications *ACS Sustainable Chem. Eng.* **2023**, in revision.
(77) Bedewy, M.; Hart, A. J. Mechanical Coupling Limits the Density and Quality of Self-Organized Carbon Nanotube Growth. *Nanoscale* **2013**, *5* (7), 2928−2937.
(78) Mauter, M. S.; Wang, Y.; Okemgbo, K. C.; Osuji, C. O.; Giannelis, E. P.; Elimelech, M. Antifouling Ultrafiltration Membranes via Post-Fabrication Grafting of Biocidal Nanomaterials. *ACS Appl. Mater. Interfaces* **2011**, *3* (8), 2861−2868.
(79) Bui, N.; Meshot, E. R.; Kim, S.; Peña, J.; Gibson, P. W.; Wu, K. J.; Fornasiero, F. Ultrabreathable and Protective Membranes with Sub-5 Nm Carbon Nanotube Pores. *Adv. Mater.* **2016**, *28* (28), 5871−5877.
(80) Li, Y.; Chen, C.; Meshot, E. R.; Buchsbaum, S. F.; Herbert, M.; Zhu, R.; Kulikov, O.; McDonald, B.; Bui, N. T. N.; Jue, M. L.; Park, S. J.; Valdez, C. A.; Hok, S.; He, Q.; Doona, C. J.; Wu, K. J.; Swager, T. M.; Fornasiero, F. Autonomously Responsive Membranes for Chemical Warfare Protection. *Adv. Funct. Mater.* **2020**, *30* (25), 2000258.
(81) Jue, M. L.; Buchsbaum, S. F.; Chen, C.; Park, S. J.; Meshot, E. R.; Wu, K. J. J.; Fornasiero, F. Ultra-Permeable Single-Walled Carbon Nanotube Membranes with Exceptional Performance at Scale. *Adv. Sci.* **2020**, *7* (24), 1−7.
(82) Plata, D. L.Carbon Nanotube Synthesis and Detection: Limiting the Environmental Impact of Novel Technologies. *PhD Thesis*; Massachusetts Institute of Technology, Cambridge, MA, 2009.
(83) Meshot, E. R.Dynamics and Limiting Mechanisms of Self-Aligned Carbon Nanotube Growth. *PhD Thesis*; University of Michigan, Ann Arbor, MI, 2012.
(84) Plata, D. L.; Hart, A. J.; Reddy, C. M.; Gschwend, P. M. Early Evaluation of Potential Environmental Impacts of Carbon Nanotube Synthesis by Chemical Vapor Deposition. *Environ. Sci. Technol.* **2009**, *43* (21), 8367−8373.
(85) Hedayati, A.; Barnett, C. J.; Swan, G.; Orbaek White, A. Chemical Recycling of Consumer-Grade Black Plastic into Electrically Conductive Carbon Nanotubes. *C (Journal of Carbon Research)* **2019**, *5* (2), 32.
(86) Shi, W.; Xue, K.; Meshot, E. R.; Plata, D. L. The Carbon Nanotube Formation Parameter Space: Data Mining and Mechanistic Understanding for Efficient Resource Use. *Green Chem.* **2017**, *19* (16), 3787−3800.
(87) Almkhelfe, H.; Carpena-Núñez, J.; Back, T. C.; Amama, P. B. Gaseous Product Mixture from Fischer−Tropsch Synthesis as an Efficient Carbon Feedstock for Low Temperature CVD Growth of Carbon Nanotube Carpets. *Nanoscale* **2016**, *8* (27), 13476−13487.
(88) Giannetto, M. J.The Roles of Alkynes in Improving the Control and Sustainability of Carbon Nanotube Synthesis. *PhD Thesis*; Yale University, New Haven, CT, 2019.
(89) Sugime, H.; Sato, T.; Nakagawa, R.; Hayashi, T.; Inoue, Y.; Noda, S. Ultra-Long Carbon Nanotube Forest via in Situ Supplements of Iron and Aluminum Vapor Sources. *Carbon N. Y* **2021**, *172*, 772−780.
(90) Buehler, M. J. Mesoscale Modeling of Mechanics of Carbon Nanotubes: Self-Assembly, Self-Folding, and Fracture. *J. Mater. Res.* **2006**, *21* (11), 2855−2869.
(91) Hart, A.; van Laake, L.; Slocum, A. Desktop Growth of Carbon-Nanotube Monoliths with In Situ Optical Imaging. *Small* **2007**, *3* (7), 1114−1114.
(92) Finnigan, B.; Jack, K.; Campbell, K.; Halley, P.; Truss, R.; Casey, P.; Cookson, D.; King, S.; Martin, D. Segmented Polyurethane Nanocomposites: Impact of Controlled Particle Size Nanofillers on the Morphological Response to Uniaxial Deformation. *Macromolecules* **2005**, *38* (17), 7386−7396.
(93) Wang, B. N.; Bennett, R. D.; Verploegen, E.; Hart, A. J.; Cohen, R. E. Quantitative Characterization of the Morphology of Multiwall Carbon Nanotube Films by Small-Angle X-Ray Scattering. *J. Phys. Chem. C* **2007**, *111* (16), 5859−5865.
(94) Faber, K.; Badaczewski, F.; Oschatz, M.; Mondin, G.; Nickel, W.; Kaskel, S.; Smarsly, B. M. In-Depth Investigation of the Carbon Microstructure of Silicon Carbide-Derived Carbons by Wide-Angle X-Ray Scattering. *J. Phys. Chem. C* **2014**, *118* (29), 15705−15715.
(95) Stein, I. Y.; Constable, A. J.; Morales-Medina, N.; Sackier, C. V.; Devoe, M. E.; Vincent, H. M.; Wardle, B. L. Structure-Mechanical Property Relations of Non-Graphitizing Pyrolytic Carbon Synthesized at Low Temperatures. *Carbon N. Y* **2017**, *117*, 411−420.
(96) Bedewy, M.; Meshot, E. R.; Reinker, M. J.; Hart, A. J. Population Growth Dynamics of Carbon Nanotubes. *ACS Nano* **2011**, *5* (11), 8974−8989.
(97) Bhalerao, G. M.; Sinha, A. K.; Srivastava, A. K.; Sathe, V.; Amarendra, G. Externally Limited Defect Generation in Multiwalled Carbon Nanotubes upon Thermal Annealing, and Possible Mechanism. *Nanotechnology* **2016**, *27* (35), 355706.
(98) Nemanich, R. J.; Solin, S. A. First- and Second-Order Raman Scattering from Finite-Size Crystals of Graphite. *Phys. Rev. B* **1979**, *20*, 392.
(99) Ferrari, A.; Robertson, J. Interpretation of Raman Spectra of Disordered and Amorphous Carbon. *Phys. Rev. B - Condens. Matter Mater. Phys.* **2000**, *61*, 14095.
(100) Bland, j. M.; Altman, D. G. Multiple Significance Tests: The Bonferroni Method. *BMJ.* **1995**, *310*, 170.

https://doi.org/10.1021/acsnanoscienceau.2c00052
ACS Nanosci. Au 2023, 3, 182−191